Bound States in the Continuum of Infinite Quality Factor in Finite Unit Cells

Hua-Wei Liang(梁华伟)[1], Yuan-Zhi Liu(刘远智)[1], Yu-Jia Zeng(曾昱嘉)[1], Yang-Jian Cai(蔡阳健)[2], and Ting-Yin Ning(宁廷银)[2*]

[1]*Key Laboratory of Optoelectronic Devices and Systems of Ministry of Education and Guangdong Province, Shenzhen University, Shenzhen 518060, China*

[2]*Shandong Provincial Engineering and Technical Center of Light Manipulations & Shandong Provincial Key Laboratory of Optics and Photonic Device, School of Physics and Electronics, Shandong Normal University, Jinan 250358, China*

(Received 26 March 2025; accepted manuscript online 24 June 2025)

A theory based on the superposition principle is developed to uncover the basic physics of wave behavior in a finite grating of N unit cells. The theory reveals that bound states in the continuum (BICs) of infinite quality factor (Q-factor) can be supported by such a grating when perfect reflection is introduced at its boundaries. If geometrical perturbations are introduced into the structure, the dark BICs transform into bright quasi-BICs with finite Q-factor, maintaining spectral characteristics nearly identical to those of quasi-BICs supported by infinite gratings. When the boundaries are replaced with high-reflectivity metallic mirrors, the Q-factor of the resonant mode is reduced to be finite; however, it can be much larger than that in the corresponding nanostructure with open boundaries and can be tuned over a large range by varying the number of unit cells or boundary conditions.

DOI: 10.1088/0256-307X/42/8/080401 CSTR: 32039.14.0256-307X.42.8.080401

Bound states in the continuum (BICs), with an infinite lifetime or infinite quality factor (Q-factor), were first proposed in quantum mechanics as peculiar solutions to the Schrödinger equation with complex artificial potentials.[1,2] The concept of BICs was then extended to various physical systems, including acoustics,[3–5] hydrodynamics,[6–8] and photonics.[9–11] Notably, BICs in photonic systems have attracted substantial attention as an emerging platform for advanced photonic applications, including low-threshold lasing,[12–14] ultrasensitive biosensing,[15–17] ultralow-level optical switching,[18,19] highly efficient nonlinear optical response,[20–23] efficient photon-pair generation,[24,25] and chiral manipulation of photons.[26]

BICs with infinite Q-factor can be realized in extended structures that are uniform or periodic in one or more directions (in-plane).[27] In such systems, the translational symmetry conserves the in-plane wave vector $k_{\parallel}$, and thus a BIC mode without radiation in the out-of-plane direction can exist inside the continuous spectrum of modes at the same $k_{\parallel}$. However, the periodic nanostructures of infinite unit cells can only be idealized theoretical constructs. In practical applications, only finitely periodic nanostructures have been fabricated.[12,13,16,21] Even if material losses, structural defects, substrate effects, etc., can all be neglected, one basic physical question remains: Can BICs with infinite Q-factor survive in an array of finite unit cells?

In previous studies, quasi-BICs or resonance modes with finite Q-factor in arrays of finite unit cells have been discussed.[28–33] The dependence of the Q-factor on the number of unit cells, N, follows a quadratic relation $Q \sim N^2$ for the symmetry-protected quasi-BICs,[28–30] and a cubic relation $Q \sim N^3$ for the accidental BICs.[31,32] However, BICs with infinite Q-factor have not been found in finite arrays due to open boundaries.

In this Letter, we establish a theory based on the superposition principle to describe the wave behavior in a finite grating of N unit cells, suggesting that it can support BICs with infinite Q-factor by introducing perfectly reflecting boundaries. The generation mechanism of the BICs is the combination of symmetry protection and constructive interference of infinitely reflected waves caused by the perfect reflection, which mimics the interference process of the BICs in infinite unit cells. The dark BICs transform into bright quasi-BICs with high Q-factor when geometrical perturbations are introduced in the grating. Two branches of standing wave modes can be supported by the structure, whose spectral behavior is nearly the same as that of quasi-BICs in infinitely periodic gratings. If the boundaries are replaced with metallic mirrors of high reflectivity, the Q-factor of the resonant mode becomes finite with or without the geometrical perturbations, which can be tuned over a large range by varying the number of unit cells or boundary conditions. The proposed theory provides an in-depth understanding of BICs in finite unit cells, which have substantial potential in nanophotonic devices.

The configuration of a one-dimensional (1D) finite grating of N unit cells with boundaries at both ends is shown in Fig. 1. The periods of the gratings with and without the perturbation are both $d = 2a + 2b$, where a

*Corresponding author. Email: ningtingyin@sdnu.edu.cn

© 2025 Chinese Physical Society and IOP Publishing Ltd. All rights, including for text and data mining, AI training, and similar technologies, are reserved.

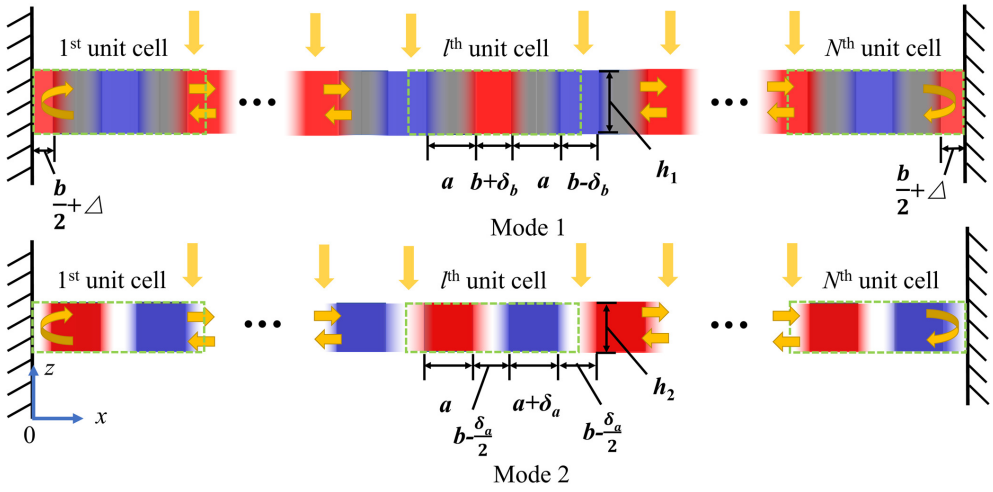

Fig. 1. Schematic diagram of a 1D finite grating with N unit cells. Two types of geometrical perturbations are introduced to obtain two different quasi-BICs. Mode 1: the widths of two dielectric (Si) nanorods in a unit cell, a, remain unchanged, while the widths of air gaps become $b+\delta_b$ and $b-\delta_b$ by introducing a position shift, δ_b. Mode 2: the widths of one dielectric (Si) nanorod and one air gap remain unchanged, while the width of the other dielectric (Si) nanorod becomes $a+\delta_a$ and the air gaps become $b-\delta_a/2$ and $b+\delta_a/2$, respectively, by introducing a perturbation, δ_a. The width of the air gaps between the outermost nanorods and the boundaries is $b/2+\Delta$ with $\Delta=0$ unless otherwise specified. The heights of dielectric (Si) nanorods are $h_1=400\,\text{nm}$ and $h_2=120\,\text{nm}$ for attaining modes 1 and 2, respectively.

and b are the initial widths of the dielectric nanorods and air gaps without perturbations. δ_b and δ_a are geometrical perturbations in structures 1 and 2, respectively. The width of the air gaps between the outermost nanorods and the boundaries is $b/2+\Delta$, with $\Delta=0$ unless otherwise specified. In the grating, counter-propagating guided waves with propagation constants of $-\beta_m$ and β_m propagate towards the left and right, respectively, where m is the order number of the guided modes. Their initial amplitudes and phases are assumed to be A_0 and 0, respectively, in all unit cells. According to the coupled-mode theory, when the guided wave from the lth unit cell arrives at the right boundary of the Nth unit cell, its electric field can be written as[34]

$$E_l = A_0 \frac{s'}{s'\cos[s'(N-l)d] + \mathrm{i}\Delta\beta_m \sin[s'(N-l)d]}, \quad (1)$$

where $s' = [(\Delta\beta_m)^2 - \kappa^*\kappa]^{1/2}$, $\Delta\beta_m = \beta_m - m\frac{2\pi}{d}$, and κ is the coupling coefficient of the two modes. If κ is much smaller than $\Delta\beta_m$, equation (1) is deduced into

$$E_l = A_0 \mathrm{e}^{-\mathrm{i}\beta_m(N-l)d}. \quad (2)$$

The interference field of the guided modes coming from the N unit cells can be expressed as

$$E'_N = A_0 \mathrm{e}^{-\mathrm{i}(N-l)\frac{\beta_m d}{2}} \frac{\sin(N\beta_m d/2)}{\sin(\beta_m d/2)}. \quad (3)$$

The fields propagate back and forth between the two boundaries, and the multiple reflections give rise to the following superposed field at the right boundary of the Nth unit cell:

$$E_{\mathrm{b}2} = E'_N \frac{r}{1-r^2\mathrm{e}^{-\mathrm{i}\beta_m 2Nd}} \mathrm{e}^{\mathrm{i}\varphi_0}. \quad (4)$$

Because the boundary may vary at different positions of the rightmost unit cell, its influence is taken into account by introducing φ_0. The complex reflection coefficient of the guided waves at either boundary is $r=|r|\mathrm{e}^{\mathrm{i}\varphi_\mathrm{r}}$, where φ_r represents the reflection-induced phase shift. Similarly, the superposed field at the left boundary is $E_{\mathrm{b}1} = E_{\mathrm{b}2}\mathrm{e}^{-\mathrm{i}2\varphi_0}$. The two waves propagating in opposite directions further interfere with each other in the grating, and the interference field can be written as

$$E = 2A_0E(x)\frac{\sin(N\beta_m d/2)}{\sin(\beta_m d/2)}\frac{r}{1-r^2\mathrm{e}^{-\mathrm{i}\beta_m 2Nd}}\mathrm{e}^{-\mathrm{i}\beta_m(N-\frac{1}{2})d}, \quad (5)$$

where $E(x)=\cos[\beta_m(\frac{Nd}{2}-x)-\varphi_0]$. See S1.1 of the Supplementary Materials (SM) for details.

When $N\to\infty$, $\beta_m = m2\pi/d$. When N is finite, a perturbation in β_m is introduced by the boundaries, i.e., the resonant field distributions should satisfy the standing wave condition $\Delta\beta_m Nd-\varphi_\mathrm{r}=(m_1-1)\pi$, where m_1 is an integer. If perfect electric conductors are adopted as the boundaries, $\varphi_\mathrm{r}\to\pi$. Therefore, two branches of BICs may be supported by the grating, and $E(x)$ can accordingly be decomposed into two components,

$$E_1(x) = \sin\left(\frac{m_1\pi x}{Nd}\right)\cos\left(\frac{m2\pi x}{d}\right), \quad (6)$$

and

$$E_2(x) = \cos\left(\frac{m_1\pi x}{Nd}\right)\sin\left(\frac{m2\pi x}{d}\right), \quad (7)$$

respectively (see S1.2 of the SM). The intensities of the two BICs can further be expressed as

$$I_1(f) = \frac{|A_0|^2\sin^2\left(\frac{m_1\pi x}{Nd}\right)\cos^2\left(\frac{m2\pi x}{d}\right)\frac{\sin^2\frac{\beta_m Nd}{2}}{\sin^2\frac{\beta_m d}{2}}F}{1+F\sin^2(\beta_m Nd-\varphi_\mathrm{r})}, \quad (8)$$

and

$$I_2(f) = \frac{|A_0|^2 \cos^2\left(\frac{m_1\pi x}{Nd}\right) \sin^2\left(\frac{m2\pi x}{d}\right) \frac{\sin^2\frac{\beta_m Nd}{2}}{\sin^2\frac{\beta_m d}{2}} F}{1 + F\sin^2(\beta_m Nd - \varphi_r)}, \quad (9)$$

where $F = 4R/(1-R)^2 \to \infty$ and $R = |r|^2 \to 1$. Consequently, both branches of the BICs are of infinite intensities at the resonant frequencies and the corresponding Q-factors are also theoretically infinite. In practical applications, even if metal mirrors of extremely high reflection are used as the boundaries, losses due to wave penetration into the metal are unavoidable. Thus, the Q-factor becomes finite, and depends on R, φ_r, N, m_1, and m (see S1.3 of the SM).

To verify the theoretical prediction, numerical simulations using the finite element method (COMSOL Multiphysics) are conducted. Two geometric structures with identical widths but different heights are employed to obtain two branches of BICs, as shown in Fig. 1. Silicon (Si) is chosen as the dielectric material. The widths of Si nanorods and air gaps without perturbations are $a = 200\,\text{nm}$ and $b = 300\,\text{nm}$, respectively. The widths of the air gaps between the outermost nanorods and the boundaries are both set as $b/2$. The refractive indices of Si and air are taken as 3.42 and 1, respectively. The detailed settings of the simulations are given in S2 of the SM. The eigenfrequency analysis was first performed to calculate the distributions of y-polarized electric fields and the Q-factor in the gratings of infinite unit cells ($N \to \infty$, no boundaries) and finite unit cells ($N = 10$) with perfect reflection at the boundaries, respectively. The BIC modes can be divided into two branches due to the introduction of the boundaries. As illustrated in the inset of Fig. 2(a), in structure 1, most of the energy of these BICs is confined within the air gaps, and the field distributions of the m_1th order modes ($m_1 = 1$, 2, and 3) agree with Eq. (6). The numerical values in the figure are the enhancement factor of the electric field and the integer $m = 1$ in these modes. On the contrary, in structure 2, most of the power of the BICs is located in the Si nanorods, and the field distributions of the m_1th order modes ($m_1 = 0$, 1, and 2) are consistent with Eq. (7), as illustrated in the inset of Fig. 2(b). Particularly, in each structure, the branch expressed by Eq. (6) or (7) can be supported and can be switched to the other by introducing several kinds of geometrical perturbations, such as a lateral shift of the cutoff positions of the boundaries by $d/4$, i.e., a nanorod with a width of $a/2$ adjoining either boundary in each structure. Similar to the BICs in the infinitely periodic nanostructure, the Q-factor of the dark BICs in the grating of finite unit cells ($N = 10$) remains infinite, which results from the combination of the symmetry protection and the constructive interference of infinite waves induced by the perfect reflection at the boundaries.

The coupling between waves in free space and the BICs with infinite Q-factor is forbidden due to symmetry protection. However, by introducing geometrical perturbations, e.g., shifting one nanorod in a unit cell away from its original position by δ_b in structure 1 or increasing the width of one rod in structure 2 by δ_a, as shown in Figs. 1(a) and 1(b), respectively, the symmetry can be broken, leading to a transition from dark BICs to bright quasi-BICs with finite Q-factors. If opposite perturbation schemes are applied to the two structures (δ_a to structure 1 and δ_b to structure 2), the Q-factor of the resonant modes approaches infinity over a broad parameter range since the mirror symmetry is conserved. Consequently, the bound states are sustained. In this case, BICs and free-space waves are decoupled. Therefore, to further investigate the interaction characteristics of this mode with free-space waves, we focus primarily on the first perturbation approach. The dependence of the Q-factor on the two geometric perturbations is calculated by eigenfrequency analysis, as illustrated in Figs. 2(a) and 2(b). When the geometrical perturbations approach zero, the Q-factor diverges toward infinity in the grating of either infinite or finite unit cells, which is the exact result of symmetry-protected BICs. Such symmetry-protected BICs are caused by the destructive interference of diffracted fields from each unit cell to free space. Along with the increase of the geometrical perturbations (δ_a or δ_b), the Q-factor of quasi-BICs in the gratings of infinite and finite ($N = 10$) unit cells both decreases, and their variation curves almost overlap. As a result, the infinite unit cells can be mimicked to obtain a high Q-factor by introducing the boundaries with perfect reflection in the

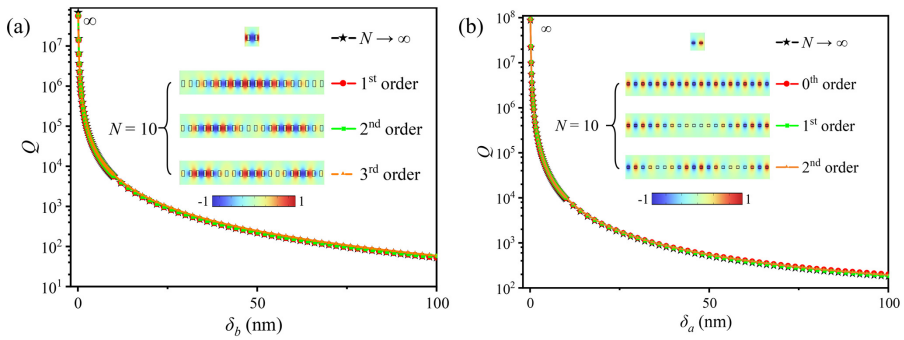

Fig. 2. Dependence of the Q-factor on (a) the geometrical perturbation δ_b in structures with a height of $h_1 = 400\,\text{nm}$ and (b) δ_a in structures with a height of $h_2 = 120\,\text{nm}$. Both gratings of infinite unit cells and finite unit cells ($N = 10$) with perfect reflection at the boundaries are considered. Insets show the distributions of y-polarized electric fields.

finite unit cells, which are similar to that of the standing wave grating with amplitude stationary in space but oscillating in time. [35]

Notably, when $N \to \infty$ and geometric perturbations vanish, the modes of infinite Q-factor in Fig. 2 are referred to as guided modes. [36] These modes reside below the light line and do not constitute BICs. However, momentum-mismatch-driven BICs are also adopted, as reported in Ref. [37], which are used to term them in this Letter. Nevertheless, adopting either "BICs" or "guided modes" as the designation does not alter our theoretical model or main conclusions.

The reflection characteristics of the infinite unit cells and finite unit cells ($N = 10$) with perfect reflection at the boundaries are then simulated. For the infinite grating with a height of $h_1 = 400\,\text{nm}$, uniform plane waves propagating in the negative z-direction are adopted as the incident light. As illustrated in Fig. 3(a), when the geometrical perturbation $\delta_b = 0$, no obvious peaks can be observed, indicating the presence of a symmetry-protected BIC. When the perturbation is introduced, a peak of Fano shape appears due to the symmetry breaking, and the peak width increases with δ_b, corresponding to the excitation of quasi-BICs. Both the Q-factor calculated from the Fano resonance and the corresponding field distributions are consistent with those obtained by the eigenfrequency analysis shown in Fig. 2(a). The dependence of the peak width on δ_b for the 10 unit cells is similar to that for the infinite grating. When the perturbation in the 10 unit cells is $\delta_b = 10\,\text{nm}$, the reflectance spectra are shown in Fig. 3(b). The initial phases of incident waves are adopted as 0, $\sin(\frac{2\pi x}{Nd})$, and $\sin(\frac{3\pi x}{Nd})$, which are used to excite the 1st, 2nd, and 3rd quasi-BICs well, respectively. The Q-factor and the field distributions of the Fano resonances are also consistent with those obtained by the eigenfrequency analysis shown in Fig. 2(a). The dependences of the Q-factor of the Fano resonances on δ_a in structures with a height of $h_2 = 120\,\text{nm}$ are shown in Fig. S2 of the SM, which are similar to those in structures with a height of $h_1 = 400\,\text{nm}$.

To evaluate the performance of the BICs in actual systems, the boundaries with perfect reflection are then replaced with aluminum (Al) mirrors. The permittivity of Al can be described by the Drude model $\varepsilon_{\text{Al}} = 1 - \omega_{\text{p}}^2/\omega(\omega - \text{i}\gamma)$, where ω is the angular frequency of light, $\omega_{\text{p}} = 2.24 \times 10^{16}\,\text{rad/s}$ and $\gamma = 1.24 \times 10^{14}\,\text{rad/s}$ are the plasma frequency and damping frequency of Al, respectively. [38] When the perturbation $\delta_b = 0\,\text{nm}$ and the width of air gaps between the outermost nanorods and the boundaries is $b/2 = 150\,\text{nm}$ in structure 1, the dependences of the Q-factor of the m_1th order BICs on the number of unit cells, N, are calculated. As shown in Fig. 4(a), the Q-factors of the three modes all increase with N, consistent with the previous results that neglect the influence of the boundaries. [28–32] However, different from earlier works, the Q-factor of the 1st mode can even exceed 10^8 when $N > 60$, which is not proportional to N^2 [28–30] or N^3. [31,32] Moreover, the variation curves of the three modes deviate

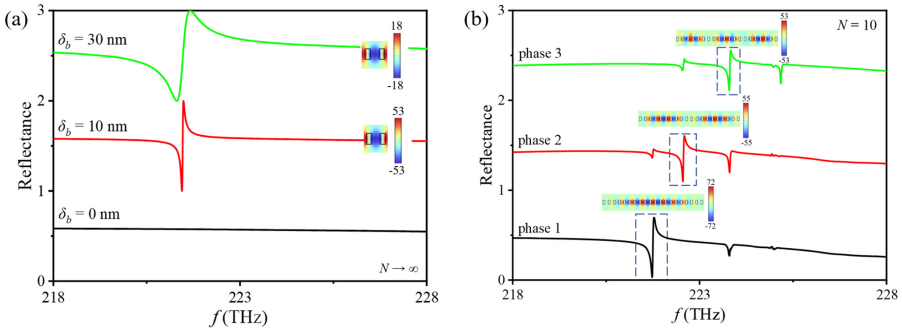

Fig. 3. Reflectance as a function of frequency under the condition of $h_1 = 400\,\text{nm}$. (a) Infinite unit cells of different δ_b. (b) Finite unit cells ($N = 10$) of $\delta_b = 10\,\text{nm}$ with perfect reflection at boundaries. Insets show the distributions of y-polarized electric fields at the corresponding resonant frequency.

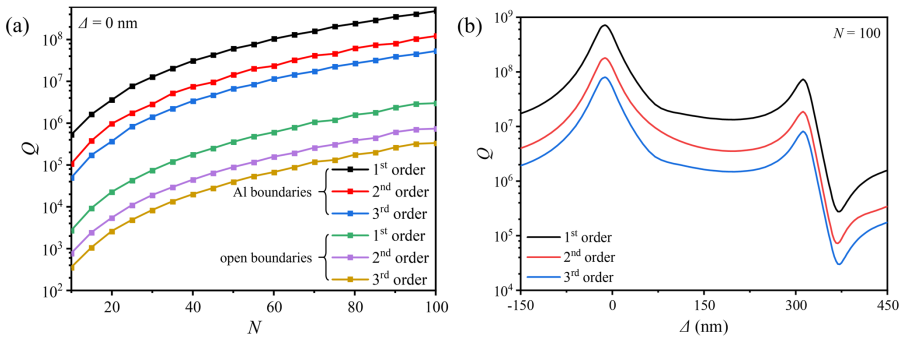

Fig. 4. Dependence of the Q-factor on (a) the number of unit cells and (b) the geometrical perturbation, Δ. The height $h_1 = 400\,\text{nm}$.

from each other, which mainly results from the difference in field distributions induced by the presence of boundaries. For comparison, the Q-factors of the resonant modes in the corresponding nanostructure with open boundaries are also presented in Fig. 4(a), which are about two orders of magnitude lower than those in the nanostructure with Al mirrors.

According to the theory in S1.3 of the SM, the Q-factor of the BICs is also dependent on the phase shift in the boundary reflection, φ_{r}. Thus, to adjust the phase equivalently, a geometric perturbation, Δ, is introduced to the width of the air gaps between the outermost nanorods and the boundaries, which is then changed from $b/2$ to $b/2+\Delta$. The dependences of the Q-factors of the three BICs in the 100 unit cells on Δ are presented in Fig. 4(b). When Δ varies from -150 to 450 nm, the fluctuation range of the Q-factor can even reach 3 to 4 orders of magnitude. The electric fields corresponding to the maximum and minimum Q-factors are presented in Figs. S3(a) and S3(b) of the SM, respectively. Although the Q-factors differ among the three BICs, their change trends are consistent, and the peaks all appear at $\Delta=-13$ nm. As shown in Fig. S4 of the SM, the Q-factor of the BICs in structure 2 is still higher than that of the corresponding nanostructure with open boundaries, even if they are located near the minimum. The fluctuation range can also reach 3 to 4 orders; however, the peaks occur at $\Delta=250$ nm. The corresponding electric fields at the peaks and valleys are shown in Fig. S5 of the SM.

Although the Q-factors of the BICs in the finite grating with metallic mirrors as their boundaries are finite, they remain dark modes due to symmetry protection. As shown in Figs. S6(a) and S7(a) in SM, when the geometrical perturbations δ_b and δ_a in structures 1 and 2 approach zero, the Q-factor reaches the peaks, all of which are finite. However, as shown in Figs. S6(b) and S7(b) of the SM, without geometrical perturbations, the coupling between waves in free space and the BICs of finite Q-factor is still forbidden, which can be excited by introducing the perturbations to break the symmetry.

In summary, a theory based on the superposition principle has been established to elucidate the fundamental physics of the wave behavior in a finite grating of N unit cells, which reveals that it can support BICs of infinite Q-factor by introducing perfect reflection at its boundaries. When the boundaries are replaced with metallic mirrors of high reflectivity, the BICs of finite Q-factor are obtained, which can be tuned over a large range by varying the number of unit cells or boundary conditions. In principle, the BICs in the two- or three-dimensional arrays of finite unit cells exhibit characteristics similar to those in the 1D grating. The results not only provide an in-depth understanding of the photonic resonances in finite unit cells but also offer significant application potential in the design and fabrication of advanced nano-photonic devices.

Acknowledgements. This work was supported by the National Natural Science Foundation of China (Grant Nos. 11874270 and 12174228) and the Shenzhen Basic Research Special Project (Grant No. JCYJ20240813141606009).

References

[1] von Neumann J and Wigner E P 1929 *Phys. Z* **30** 465
[2] Stillinger F H and Herrick D R 1975 *Phys. Rev. A* **11** 446
[3] Evans D V, Levitin M, and Vassiliev D 1994 *J. Fluid Mech.* **261** 21
[4] Lyapina A A, Maksimov D N, Pilipchuk A S, and Sadreev A F 2015 *J. Fluid Mech.* **780** 370
[5] Deriy I, Toftul I, Petrov M, and Bogdanov A 2022 *Phys. Rev. Lett.* **128** 084301
[6] McIver M 1996 *J. Fluid Mech.* **315** 257
[7] McIver M 2000 *Proc. R. Soc. A* **456** 1851
[8] Porter R 2002 *Proc. R. Soc. A* **458** 607
[9] Marinica D C, Borisov A G, and Shabanov S V 2008 *Phys. Rev. Lett.* **100** 183902
[10] Bulgakov E N and Sadreev A F 2008 *Phys. Rev. B* **78** 075105
[11] Song Q J, Dai S W, Han D Z, Zhang Z Q, Chan C T, and Zi J 2021 *Chin. Phys. Lett.* **38** 084203
[12] Kodigala A, Lepetit T, Gu Q, Bahari B, Fainman Y, and Kante B 2017 *Nature* **541** 196
[13] Zhang X D, Liu Y L, Han J C, Kivshar Y, and Song Q G 2022 *Science* **377** 1215
[14] Riabov D, Gladkov R, Pashina O, Bogdanov A, and Makarov S 2024 *Laser Photon. Rev.* **18** 2300829
[15] Chen Y, Zhao C, Zhang Y Z, and Qiu C W 2020 *Nano Lett.* **20** 8696
[16] Yesilkoy F, Arvelo E R, Jahani Y, Liu M K, Tittl A, Cevher V, Kivshar Y, and Altug H 2019 *Nat. Photon.* **13** 390
[17] Li Z L, Nie G Z, Chen Z Q, Zhan S P, and Lan L F 2024 *Opt. Lett.* **49** 3380
[18] Karl N, Vabishchevich P P, Liu S, Sinclair M B, Keeler G A, Peake G M, and Brener I 2019 *Appl. Phys. Lett.* **115** 141103
[19] Han Z H and Cai Y J 2021 *Opt. Lett.* **46** 524
[20] Carletti L, Koshelev K, De Angelis C, and Kivshar Y 2018 *Phys. Rev. Lett.* **121** 033903
[21] Liu Z J, Xu Y, Lin Y, Xiang J, Feng T H, Cao Q T, Li J T, Lan S, and Liu J 2019 *Phys. Rev. Lett.* **123** 253901
[22] Ning T Y, Li X, Zhao Y, Yin L Y, Huo Y Y, Zhao L N, and Yue Q Y 2020 *Opt. Express* **28** 34024
[23] Liu T T, Qin M B, Wu F, and Xiao S Y 2023 *Phys. Rev. B* **107** 075441
[24] Parry M, Mazzanti A, Poddubny A, Valle G D, Neshev D N, and Sukhorukov A A 2021 *Adv. Photon.* **3** 055001
[25] Liu T T, Qin M B, Feng S Q, Tu X, Guo T J, Wu F, and Xiao S Y 2024 *Phys. Rev. B* **109** 155424
[26] Overvig A, Yu N F, and Alú A 2021 *Phys. Rev. Lett.* **126** 073001
[27] Hsu C W, Zhen B, Stone A D, Joannopoulos J D, and Soljacic M 2016 *Nat. Rev. Mater.* **1** 16048
[28] Taghizadeh A and Chung I S 2017 *Appl. Phys. Lett.* **111** 031114
[29] Bulgakov E N and Sadreev A F 2017 *J. Opt. Soc. Am. A* **34** 949
[30] Sadrieva Z F, Belyakov M A, Balezin M A, Kapitanova P V, Nenasheva E A, Sadreev A F, and Bogdanov A A 2019 *Phys. Rev. A* **99** 053804
[31] Bulgakov E N and Sadreev A F 2019 *Phys. Rev. A* **99** 033851

[32] Sidorenko M S, Sergaeva O N, Sadrieva Z F, Roques-Carmes C, Muraev P S, Maksimov D N, and Bogdanov A A 2021 *Phys. Rev. Appl.* **15** 034041

[33] Bulgakov E, Shadrina G, Sadreev A, and Pichugin K 2023 *Phys. Rev. B* **108** 125303

[34] Yariv A 2007 *Photonics: optical electronics in modern communications, 6th edn.* (New York: Oxford University Press)

[35] Horsley S A R and Pendry J B 2024 *Phys. Rev. Lett.* **133** 156903

[36] Sun K, Wei H, Chen W, Chen Y, Cai Y, Qiu C W, and Han Z 2024 *Phys. Rev. B* **109** 085426

[37] Wu F, Qi X, Qin M, Luo M, Long Y, Wu J, Sun Y, Jiang H, Liu T, Xiao S, and Chen H 2024 *Phys. Rev. B* **109** 085436

[38] Ordal M A, Bell R J, Alexander R W, Long L L, and Querry M R 1985 *Appl. Opt.* **24** 4493